Discrete Breathers in a Forced-Damped Array of Coupled Pendula: Modeling, Computation, and Experiment

J. Cuevas,[1] L. Q. English,[2] P. G. Kevrekidis,[3] and M. Anderson[2]

[1]*Departamento de Física Aplicada I. Escuela Universitaria Politécnica, Universidad de Sevilla. C/ Virgen de África, 7, 41011 Sevilla, Spain*

[2]*Department of Physics & Astronomy, Dickinson College, Carlisle, Pennsylvania 17013, USA*

[3]*Department of Mathematics and Statistics, University of Massachusetts, Amherst, Massachusetts 01003-4515, USA*

(Received 12 February 2009; published 2 June 2009)

In this work, we present a mechanical example of an *experimental realization* of a stability reversal between on-site and intersite centered localized modes. A corresponding realization of a vanishing of the Peierls-Nabarro barrier allows for an experimentally observed enhanced mobility of the localized modes near the reversal point. These features are supported by detailed numerical computations of the stability and mobility of the discrete breathers in this system of forced and damped coupled pendula. Furthermore, additional exotic features of the relevant model, such as dark breathers are briefly discussed.

DOI: 10.1103/PhysRevLett.102.224101 PACS numbers: 05.45.Yv, 63.20.Pw

Introduction.—Discrete breathers (also referred to as intrinsic localized modes or ILMs) have been the focal point of numerous studies over the past two decades (for a recent review of the relevant activity see, e.g., [1]). Such localized modes of nonlinear lattices have been found to be fairly generic and constitute a new paradigm in nonlinear science whose applications extend to physics and chemistry, as well as to biology. Their original proposal in the broadly applicable context of anharmonic lattices [2,3] and subsequent theoretical analysis (including the rigorous proof of their existence under appropriate conditions [4]) has led to numerous experimental realizations ranging from optical waveguides and photorefractive crystals to micromechanical cantilever arrays and Josephson junctions, as well as to Bose-Einstein condensates and layered antiferromagnets, among many others [1,5].

Typically, these ILMs come into two principal varieties in one-dimensional chains, namely, the on-site centered (also referred to as one-site) modes [2] and the intersite centered ones (two-site modes) [3]. In the simplest ones among the relevant models supporting such structures, either the former, or the latter modes are stable, and this property is maintained when relevant parameters, such as the lattice spacing, are varied [6]. However, more recently it has been illustrated that stability exchanges are theoretically possible between these modes [7], which result either in a true [8] or approximate [9] vanishing of the, so-called, Peierls-Nabarro barrier, namely, the energy difference between them. This vanishing is, in turn, relevant in that it enables the localized modes to move along the lattice without facing such an energy barrier, thereby enhancing their mobility [7,8].

Our aim in the present work is to demonstrate an *experimental realization* of a setting which enables such *stability reversals* between on-site and intersite modes, namely, an array of pendula under the action of driving and damping. A detailed analysis illustrates such stability exchanges to occur numerically, and the experimental findings validate this result. Furthermore, enhanced mobility of the localized modes is observed experimentally and computationally near the exchange point and additional theoretically interesting features of the model are predicted (in a regime that is not currently accessible experimentally to us). Herein, we will operate in a moderate discreteness regime, namely, one that is neither strongly discrete (where breathers consist of very few sites), nor nearly continuum (where no distinction between one- and two-sites would be discernible). The continuum limit of the models considered has been examined in detail at the level of sine-Gordon [10] and at the small pendulum angles limit of the nonlinear Schrödinger equation [11]. Our presentation is as follows. In the next section, we explain the experimental setup, followed by the theoretical or numerical setup. We close the Letter with a detailed discussion of the results, as well as some potential future directions.

Experimental setup.—We investigate a driven and damped chain of pendula each comprised of a rod of mass m and length L ending in a weight of mass M (see, e.g., the top panel of Fig. 1). They are suspended along a line by a taut piano wire stretched across a metal frame and connected via springs, as in [12]. The system is driven sinusoidally along a horizontal direction with an adjustable amplitude A and a tunable frequency ω_d. The resulting dynamics of the pendulum chain is recorded by an overhead camera, and individual frames can be used to extract pendulum angles. The governing equations of motion for a pendulum in the chain take into account the detailed effects of driving and damping

$$\ddot{\theta}_n + \omega_0^2 \sin\theta_n - \left(\frac{\beta}{I}\right)\Delta_2\theta_n + \frac{\gamma_1}{I}\dot{\theta}_n - \frac{\gamma_2}{I}\Delta_2\dot{\theta}_n + F\omega_d^2\cos(\omega_d t)\cos(\theta_n) = 0 \qquad (1)$$

with $I = ML^2 + \frac{1}{3}mL^2$, $\omega_0^2 = \frac{1}{I}(mg\frac{L}{2} + MgL)$, and $F = \frac{A\omega_0^2}{g}$,

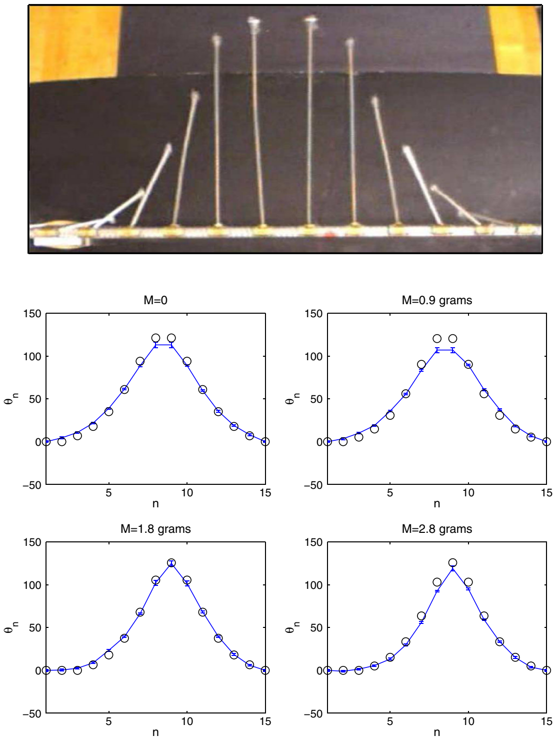

FIG. 1 (color online). Snapshot illustrating the experimental setup and the observation of an intersite breather (top panel), and comparison of experimental and numerical profiles of stable intersite breathers (middle panels) and on-site breathers (bottom panels). In all cases, $A = 1.12$ cm and $\omega_b = 0.87$. Circles represent the numerical results whereas the full lines with error bars correspond to the experimental profiles.

while Δ_2 represents the discrete Laplacian. Here, g is 9.80 N/kg, and β denotes the torsional spring constant. The nature of damping in the system warrants closer inspection. Two types of friction are present in the experiment—an on-site and an intersite one. The on-site component (of prefactor γ_1) comes from air drag as well as contact friction at the suspension points. The intersite component (of prefactor γ_2) has its origin in the energy dissipation due to the twisting of the springs, and it should be related to angle differences between neighboring springs. This draws interesting parallels to the lattice turbulence models of [13] and recent models of granular crystals [14]. Equation (1) can be nondimensionalized by introducing the following parameters: $\omega_b = \frac{\omega_d}{\omega_0}$, $C = \frac{\beta}{I\omega_0^2}$, and $\alpha = \frac{\gamma}{I\omega_0}$ (F is already dimensionless).

This model is similar to that of [15], but here the driving term depends on the angular displacement at each lattice site and on the driving frequency. The definition of C suggests two experimental ways of adjusting this parameter. For gross adjustment, one can change the springs between the pendula modifying the torsional stiffness and coupling β. A finer (and more convenient) way of varying C is via I and ω_0. This can be done most easily by changing the end mass M which affects I and ω_0. Note that by changing ω_0, ω_b and F are also affected.

The on-site damping constant, γ_1, was measured using just one isolated pendulum, tracking its amplitude decay over time (which yields γ_1/I). Incidentally, γ_1 was measured for a number of end masses, M, and found to be approximately independent of end mass for $M < 10$ g.

The parameter γ_2 was estimated as follows. Starting with three pendula connected in a line via springs, the two outer ones are held fixed vertically, and the amplitude decay of the center pendulum is tracked. The exponential decay constant thus obtained is then divided by the angular velocity ω for this mode (in the linear regime), which can be measured independently. This number corresponds to an effective α, and it is larger than $\alpha_1 = \gamma_1/(I\omega_0)$.

Experimental values used were $\beta = 0.0165$ Nm/rad, $\gamma_1 = 284\ \mathrm{g\,cm^2/s}$, $\gamma_2 = 70\ \mathrm{g\,cm^2/s}$, $L = 25.4$ cm, $m = 13$ g, $A = 1.12$ cm.

Theoretical or numerical setup.—We consider the breather existence and stability in the (nondimensional) equations of motion. Our computations start at the anticontinuous (AC) limit ($C = 0$), using the two (different amplitude) attractors of an uncoupled pendulum. Breathers close to the AC limit only exist if there are two coexisting attractors of the single driven and damped pendulum—both phase-locked to the external driving. The highest-amplitude attractor will correspond to the excited breather site(s) whereas the smallest-amplitude one will be chosen for the low-amplitude background. Then, the breather will be a collective oscillation at the driving frequency, ω_b. For the analyzed parameter range, the attractors oscillate in antiphase. As a consequence, the excited site of the breather oscillates in antiphase with respect to the tails, in agreement with the experimental observations of [12]. Upon creation at the AC limit, such solutions have been continued for arbitrary $C \neq 0$, through a path-following scheme in the real space, as proposed in [16]; this method allows us to identify both stable and unstable solutions.

The linear stability of the ensuing discrete breathers is studied by means of a Floquet analysis. To this end, we add a small perturbation ξ_n to the breather solution leading to the following equation for the perturbations:

$$\ddot{\xi}_n + \alpha\dot{\xi}_n + h(t;\theta_n(t))\xi_n - C\Delta_2\xi_n - \alpha_2\Delta_2\dot{\xi}_n = 0 \quad (2)$$

with $h(t;\theta_n(t)) = \cos\theta_n(t) - F\omega_b^2\cos(\omega_b t)\sin\theta_n(t)$.

Stability analysis is performed by diagonalizing the monodromy matrix $\mathcal{M}$, which relates the perturbation at $t = 0$ to that at $t = T$:

$$\begin{pmatrix} \xi_n(T) \\ \dot{\xi}_n(T) \end{pmatrix} = \mathcal{M}\begin{pmatrix} \xi_n(0) \\ \dot{\xi}_n(0) \end{pmatrix}. \quad (3)$$

The linear stability of breathers requires that the monodromy eigenvalues (Floquet multipliers) must be inside (or at) the unit circle; see, e.g., [17,18] for details. Because of the intersite damping, only one property (implied by the real character of the monodromy) can be extracted for the multipliers, which is that they appear in complex conjugated pairs (λ, λ^*).

Results and discussion.—Let us start by comparing typical experimental and numerical breather profiles. Subsequently, we will explore the regions in parameter space where the two types of breathers are stable. Finally, we briefly discuss additional interesting system features such as moving and dark breathers.

In order to compare with experimental profiles, we choose a chain with 13 pendula and fixed-end boundary conditions. Figure 1 details the experiment-theory comparison. The circles indicate computed values and the line shows the experimental profile; experimental uncertainties are indicated by the error bars. The uncertainty for angles higher than 100° is ± 3 whereas it is ± 1 if the angles are smaller. An exchange of stability is identified *both* numerically and experimentally: for small masses, two-site breathers are stable whereas for larger masses, one-site breathers become stable.

The experimentally accessible parameters are M, ω_b, and F (via A). To explore breather stability and symmetry more fully, we numerically generate two-parameter diagrams for a larger-sized array. To this end, we have chosen a chain of $N = 41$ pendula (so that boundary effects are of lesser importance). Figure 2(a) illustrates the breather stability for fixed $A = 1.12$ cm (left panel where M and ω_b are varied). We observe that as M is increased, at a given ω_b, an exchange of stability bifurcation is observed: the one-site breather gains stability, and (practically) simultaneously the two-site breather solution loses stability. Conversely, for a given M, an exchange of stability can be induced by varying ω_b. Above a critical value (≈ 0.875), the system experiences a Naimark-Sacker (NS) bifurcation (viz. generalized Hopf or Hopf bifurcation of periodic orbits) leading to the eventual breather disappearance. For driver frequencies ω_b below a critical lower value, we observe the nonexistence of any kind of breather (even unstable ones). Notice that the four dots in Fig. 2(a) correspond to the parameters of Fig. 1 with $M = 0$ g and $M = 0.9$ g falling into the two-site regime at $\omega_b = 0.87$, whereas $M = 1.8$ g and $M = 2.8$ g are in the one-site regime.

According to the figure, the stability exchange can also be initiated by varying the driver frequency at a fixed end mass, and this was also tested experimentally. For $M = 1.8$ g, the one-site ILM is found to be stable down to $\omega_b \cong 0.83$. At that point, a transition to two-site ILM appears to be initiated. The resulting two-site ILM is, however, difficult to stabilize in the system of 13 pendula, and it usually decays within 5–10 periods. The observed transition frequency agrees reasonably well with the predicted value of 0.805. At $M = 1.2$ g, the transition can be observed more clearly. The on-site breather prevails at $\omega_b = 0.96$. Below $\omega_b = 0.91$ the intersite breather is stable; the predicted value is, in this case, 0.852. The NS-bifurcation at larger ω_b is also clearly observed experimentally but for end masses above $M = 6.8$ g (see also [12]).

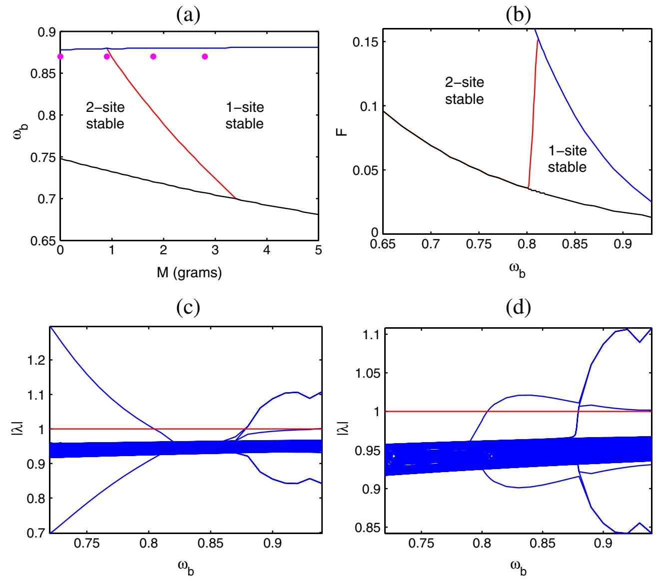

FIG. 2 (color online). Top: Numerical two-parameter planes for (left) fixed $A = 1.12$ cm and (right) fixed $M = 1.8$ g. Full circles in the left panel correspond to the solutions shown in Fig. 1. Bottom: numerically computed moduli of Floquet multipliers (indicating stability, when they are all smaller than 1) for (left) one-site and (right) two-site breathers. In this case, $F = 0.06$ and $M = 1.8$ g are fixed, while ω_b is variable. An exchange of stability bifurcation is observed for $\omega_b \in (0.804, 0.805)$. In both cases, the bifurcation arising for higher ω_b is a Naimark-Sacker one.

In Fig. 2(b), a F-ω_b plane for fixed $M = 1.8$ g is depicted. Here we see that two-site breathers are stable for small ω_b with an exchange of stability bifurcation taking place in a narrow range of frequencies around $\omega_b = 0.81$. Below $\omega_b = 0.65$ breathers are NS-unstable. Notice, again, that for small values of F breathers cannot be found. Figures 2(c) and 2(d) show a typical parametric dependence of the Floquet exponents for two different configurations.

The above stability exchanges between the two principal configurations (and the corresponding vanishing of the energy barrier between them) renders credible the scenario of breather mobility near such parameter sets [7,8]. Such mobility has been observed (even in fairly large lattices with ≈ 100 sites) and typically requires appropriately large values of F. A typical example of such a traveling breather for $F = 0.15$ is depicted in Fig. 3 ($\omega_b = 0.66$ and $M = 3.8$ g). Such observations are in agreement with experimental indications of mobility (albeit admittedly in the fairly short experimental lattice), as shown in the bottom panel of the Fig. 3. The experimental parameters are $M = 1.8$ g ($C = 0.8$) and $\omega_b = 0.87$. In this regime, a stationary ILM can be made to move easily by bringing a fixed boundary into the wings of the ILM; in response, the ILM will move away from the boundary. The figure depicts an ILM repelled from the left boundary; it moves fairly quickly at first—alternating between one-site and two-site symmetry—then slows down and finally comes to rest

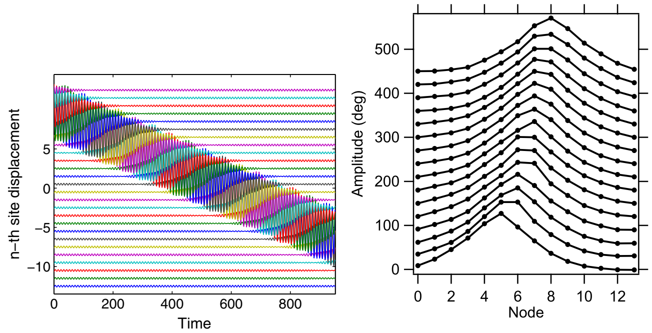

FIG. 3 (color online). (Left panel) Numerical (for $F = 0.15$) and (right panel) experimental examples of breather mobility. In the left panel, $M = 3.8$ g and $\omega_b = 0.66$, while the right panel example is for $M = 1.8$ g and $\omega_b = 0.87$. The vertically stacked experimental profiles are spaced one period apart.

three sites over. To demonstrate another interesting feature of the model, let us now investigate the existence and stability of *dark breathers*. In Ref. [19] the existence of dark breathers in the dissipative Klein-Gordon lattice with nonparametric driving was demonstrated. Figure 4 shows the existence and stability range of dark breathers. As shown, the range of stability of dark breathers is somewhat limited. We have varied parameters ω_b and C for fixed $\gamma = 0.001$, $\gamma_2 = 0$ and $F = 0.10$. For small ω_b, the dark breathers are exponentially unstable and lead to dark-localized structures. For large ω_b pseudodark (i.e., not asymptoting to a constant background state) breathers are stable instead; see the bottom panels of Fig. 4. For ω_b above the range shown in the figure, the breathers experience a NS bifurcation. This instability is, however, small and system-size dependent. It was numerically found that dark breathers do not exist for $\omega_b \gtrsim 0.95$, while for $C > 0.012$, stable dark breathers also do not exist—a constraint which in our present experimental setting inhibits the formation of such coherent structures.

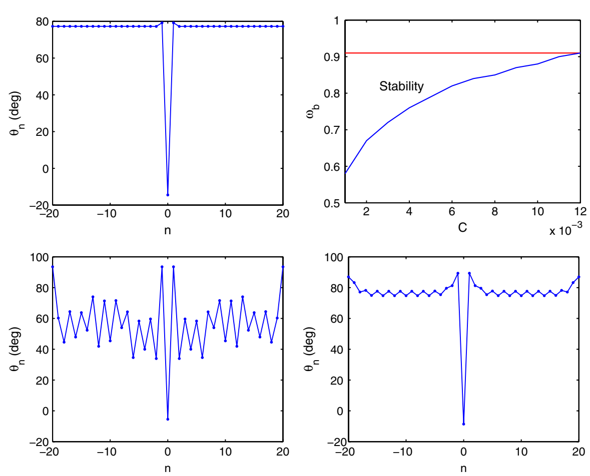

FIG. 4 (color online). (Top panels) Dark breather profile for $C = 0.01$ and $\omega_b = 0.9$ (left) and ω_b-C plane for the values specified in the text. (Bottom panels) Example of pseudodark (i.e., not asymptoting to a constant background) breathers with $C = 0.01$ which are stable in the range where "real" dark breathers are exponentially-unstable [(left) $\omega_b = 0.8$ and (right) $\omega_b = 0.86$].

Conclusions.—We have illustrated that the setting of damped and driven coupled pendula is an ideal playground for showcasing many interesting features of discrete breathers. In particular, in addition to bearing unusual model features, such as intersite dissipation, this system exhibits complex stability properties evidenced by stability exchanges between on-site and intersite configurations. These, in turn, lead to interesting breather dynamics, including the potential for mobility of such localized excitations. Our numerical results based on the proposed model were found to be in excellent qualitative and good quantitative agreement with the experimental findings. Determining whether multisite excitations are possible would be among the natural extensions of the present work.

This research has been supported by a Research Corporation grant, the Ministerio de Ciencia e Innovación of Spain (FIS2008-04848), and by NSF-CAREER (NSF-DMS-0349023) and NSF-DMS-0806762.

[1] S. Flach and A. Gorbach, Phys. Rep. **467**, 1 (2008).
[2] A. J. Sievers and S. Takeno, Phys. Rev. Lett. **61**, 970 (1988).
[3] J. B. Page, Phys. Rev. B **41**, 7835 (1990).
[4] R. S. MacKay and S. Aubry, Nonlinearity**7**, 1623 (1994).
[5] D. K. Campbell, S. Flach, and Yu. S. Kivshar, Phys. Today **57**, No. 1, 43 (2004).
[6] T. Kapitula and P. Kevrekidis, Nonlinearity **14**, 533 (2001).
[7] L. Hadzievski *et al.*, Phys. Rev. Lett. **93**, 033901 (2004).
[8] T. R. Melvin *et al.*, Phys. Rev. Lett. **97**, 124101 (2006).
[9] R. Carretero-González *et al.*, Physica (Amsterdam) **216D**, 77 (2006).
[10] D. Cai, A. R. Bishop, and A. Sanchez, Phys. Rev. E **48**, 1447 (1993); J. C. Ariyasu and A. R. Bishop, Phys. Rev. B **35**, 3207 (1987).
[11] I. V. Barashenkov and Yu. S. Smirnov, Phys. Rev. E **54**, 5707 (1996); I. V. Barashenkov, Yu. S. Smirnov, and N. V. Alexeeva, Phys. Rev. E **57**, 2350 (1998); I. V. Barashenkov and E. V. Zemlyanaya, Physica (Amsterdam) **132D**, 363 (1999).
[12] R. Basu-Thakur, L. Q. English, and A. J. Sievers, J. Phys. D **41**, 015503 (2008).
[13] M. Peyrard and I. Daumont, Europhys. Lett. **59**, 834 (2002).
[14] R. Carretero-González *et al.*. Phys. Rev. Lett. **102**, 024102 (2009).
[15] J. L. Marín *et al.*, Phys. Rev. E **63**, 066603 (2001); P. J. Martínez *et al.*, Chaos **13**, 610 (2003).
[16] J. L. Marín and S. Aubry, Nonlinearity **9**, 1501 (1996).
[17] S. Aubry, Physica (Amsterdam) **103D**, 201 (1997).
[18] J. F. R. Archilla *et al.*, Physica (Amsterdam) **180D**, 235 (2003); J. Cuevas, J. F. R. Archilla, and F. R. Romero, Nonlinearity **18**, 769 (2005).
[19] A. Álvarez *et al.*, New J. Phys. **4**, 72 (2002).